



ORIGINAL ARTICLE

Preparation and characterization of a novel magnetized nanosphere as a carrier system for drug delivery using *Plantago ovata* Forssk. hydrogel combined with mefenamic acid as the drug model



Behnam Mahdavi^{a,*}, Sareh Hosseini^a, Majid Mohammadhosseini^b,
Mohammad Mehrshad^c

^a Department of Chemistry, Faculty of Science, Hakim Sabzevari University, 96179-76487 Sabzevar, Iran

^b Department of Chemistry, College of Basic Science, Shahrood Branch, Islamic Azad University, Shahrood, Iran

^c Department of Chemistry, Sabzevar Branch, Islamic Azad University, Sabzevar, Iran

Received 4 February 2022; accepted 12 July 2022

Available online 16 July 2022

KEYWORDS

Drug delivery, magnetized hydrogel;
Mefenamic acid;
Plantago ovata Forssk

Abstract The aim of the present study was to magnetize *Plantago ovata* Forssk. hydrogel and produce a nanosphere system to carrier mefenamic acid as the drug model. For this propose, *P. ovata* seeds hydrogel (POSH) was extracted and magnetized by Fe₃O₄ being functionalized using tetraethyl orthosilicate and trimethoxyvinylsilane. Thereafter, mefenamic acid (MFA) was loaded on the carrier system. The final product, as the magnetic drug loaded nanosphere (Fe/POSH/MFA), was fully characterized through different techniques involving X-ray diffraction (XRD), scanning electron microscopy (SEM), vibrating-sample magnetometer (VSM), thermal gravimetric analysis (TGA), dynamic light scattering (DLS), and FT-IR spectroscopy. The results confirmed the successful production of the drug loaded nanosphere system with particles magnetization of 25 emu/g over a range size of 40–50 nm. However, the size distribution less than 100 nm was measured through DLS analysis. The hydrogel showed a pH sensitivity swelling behavior representing the best efficacy at pH 7.4. The efficiency of the drug encapsulation was found to be 64.35%. The drug releasing was studied using a dialysis bag at pH = 7.4. The highest *in vitro* drug releasing was found to be 57.3 ± 0.6% after 72 h, as well. The findings of the current report account for the potential use

* Corresponding author.

E-mail address: b.mahdavi@hsu.ac.ir (B. Mahdavi).

Peer review under responsibility of King Saud University.



Production and hosting by Elsevier

of *P. ovata* hydrogel as an effective delivery system for encapsulation of water insoluble basic drugs, e.g., MFA in a magnetized carrier system.

© 2022 The Authors. Published by Elsevier B.V. on behalf of King Saud University. This is an open access article under the CC BY-NC-ND license (<http://creativecommons.org/licenses/by-nc-nd/4.0/>).

1. Introduction

Plantago ovata Forssk or Psyllium is an annual plant from the *Plantago* genus and is widely grown in India and Iran (Ladjevardi et al., 2015). A literature survey demonstrates that the plant seeds husk has been used as a dietary fiber supplement to promote the regulation of large bowel function for many years. Furthermore, this herbal species is frequently prescribed as a demulcent, emollient, and laxative agent in the traditional medicine of various regions of the world. The plant is also effective in the treatment of dysentery, inflamed membranes of the intestinal canal, constipation, high cholesterol, colon cancer, diarrhea, and diabetes (Ahmadi et al., 2012). Psyllium takes several advantages in pharmaceutical and food industries. In this sense, a variety of promising applications of this plant could be attributed to Psyllium seed hydrogel (Ahmadi et al., 2012). In general, the plants seeds hydrogels are classified into two categories involving pectin-rich and hemicellulose-rich hydrogels (Yu et al., 2017). Arabinoxylans are the main constituents of Psyllium seed hydrogel. These carbohydrate compounds consist of a xylan backbone with a variety of side chains of xylose and arabinose residues. Due to the formation of a strong gel, this polysaccharide considerably improves the consistency and stability of the natural systems (Ladjevardi et al., 2015, Yu et al., 2017).

Due to availability, inexpensiveness and appearing as a renewable polymer, Psyllium seed hydrogel is known as an excellent candidate for potential usage in some environmental and biomedical fields (Wadhera et al., 2020). The presence of bioactive polysaccharide in Psyllium hydrogel makes it as a potent agent to treat constipation, colon cancer, diarrhea, high cholesterol, diabetes and inflammation bowel diseases – ulcerative colitis (Ahmadi et al., 2012). As being documented, the Psyllium husk, is responsible for both laxative and cholesterol-lowering activities (Fischer et al., 2004). *Plantago* Psyllium mucilage with ingredients of protein, sugar, fat, and tannin with carboxylic and hydroxylic functional groups shows remarkable capability to adsorb some pollutants (Mirzaei and Javanbakht 2019). Hydrogels with hydroxyl and quaternary ammonium functional groups are able to capture and kill some bacteria through electrostatic forces, Van der Waals forces, and hydrophobic interactions (Qi et al., 2022).

So far, various natural or synthetic polymers have been successfully used to develop nanoparticles in drug delivery systems (Buhecha et al., 2019). Hydrogels are three-dimensional, hydrophilic, and polymeric networks and have a wide range of applications in tissue engineering, food, and pharmaceutical technology. It has been shown that hydrogels exhibit a remarkable tendency to absorb large quantities of water to swell and this unique flexibility and biocompatibility make them as a basic component in diverse drug delivery-based systems (Iqbal et al., 2011, Ghorpade et al., 2019, Jeong et al., 2019). Nontoxicity and biodegradability of naturally occurring ionic polysaccharides such as pectin carrageenan, chitosan or Psyllium husk make them suitable for encapsulation of a wide variety of biologically active agents (-Belščak-Cvitanović et al., 2015). Besides, the drug delivery systems consist of biocompatible structures in which the drug is encapsulated and then released. In these systems, carriers can be inorganic materials, e.g., metal-organic frameworks, carbon nanotubes, zeolites, and silica or organic materials, e.g., polymers, micelles and dendrimers containing different functional groups (Zauska et al., 2021). Mesoporous silica nanoparticles are considered as new carrier systems in drug delivery because of their biocompatibility, high porosity and also ability to host large amount of active pharmaceutical ingredients (Brezoiu et al., 2019). The most well-known types of this class of materials include

the MCM-41(with hexagonal structure), MCM-48 (with cubic structure), and MCM-50 (with lamellar structure). SBA-15 is another system with uniform hexagonal pores and a tunable diameter (Abukhadra et al., 2020, Costa et al., 2020, Jiang et al., 2020, Yuan et al., 2020).

In literature, various synthetic and natural polymers have been used in drug delivery-based applications (Buhecha et al., 2019) among which, cellulose and its water-soluble derivatives are increasingly preferred mostly due to their low cost and abundance (Ghorpade et al., 2019). Hydrogels are identified as effective supporters to carry magnetic nanoparticles. Besides, the low cost and excellent biocompatibility are the other advantages of hydrogels (Cheng et al., 2021, Pan et al., 2021). The potential use of hydrogel containing magnetic nanoparticles is a proper approach for targeted and controlled drug delivery. Furthermore, the excellent drug-loading capability is another advantage of the magnetic-hydrogel system (Wang et al., 2019).

2-(2,3-Dimethylphenyl) aminobenzoic or mefenamic acid (MFA) is an anthranilic acid derivative. In fact, MFA is a non-steroidal anti-inflammatory drug and is also effective to relieve severe headaches as well as muscle and dental pains. Furthermore, MFA has been reported as a potent analgesic and anti-inflammatory agent in the treatment of osteoarthritis, rheumatoid arthritis, and menorrhagia (Tantiwattanakul and Taneepanichskul 2004, Zisimopoulos et al., 2009, Iyer and Gogate 2017). However, poor solubility, high hydrophobicity, and tendency to stick to surfaces are the major drawbacks of MFA to granulate, tableting, and dissolution (Antonio and Maggio 2018). Due to slow dissolution rate, the drug needs more time to dissolve in the gastrointestinal fluid and this can affect the bioavailability and therapeutic efficacy of MFA (Jarrar et al., 2017).

In this study, we have prepared a novel nanocomposite in form of magnetic-Psyllium hydrogel nanosphere for controlled drug delivery using a core-shell system. The iron oxide was the core that was coated by functionalized silica. Silica aerogels, as an inorganic component have sustained drug release behavior because of the relevant structural properties. These compounds can be made of metal alkoxides such as tetraethyl orthosilicate (TEOS), trimethyl orthosilicate (TMOS), or inorganic metal salts such as sodium silicate (Boccardi et al., 2019, Porrhng et al., 2021). Silica aerogels can be functionalized by non-hydrolysable methyl and vinyl groups of methyltrimethoxysilane (MTMS) and vinyltrimethoxysilane (VTMS). These precursors are non-polar and hence have very little and negligible affinity towards the polar molecules in the pores of the gel – the alcoholic solvent and water (Vareda et al., 2018). To study the ability of the prepared magnetized Psyllium hydrogel in drug delivery, mefenamic acid was used to be loaded onto the prepared system as a drug model. Various characterization techniques including FT-IR, XRD, SEM, TGA, and VSM were used to investigate the structure and composition of the magnetized nanosphere as the carrier system. The drug releasing trend was also evaluated under different conditions of some relevant experimental variables, e.g., pH and temperature using UV/Vis spectroscopy.

2. Experimental

2.1. Material and instrumentation

Tetraethyl orthosilicate (TEOS), methacrylic acid (MAA), ethylene glycol dimethacrylate (EGDMA), trimethoxyvinylsi-

lane (TMVS), cetyl trimethylammonium bromide (CTAB) and A.A'- azoisobutyronitrile (AIBN) were purchased from Sigma-Aldrich.

Different techniques were used to characterize the yields and products in this research. A Shimadzu FT-IR 8400 recorded the FT-IR spectra (400–4000 cm^{-1} and KBr disc); MIRA3TESCAN-XMU reported the FE-SEM Images; the XRD patterns was obtained in the 2θ scale (20–80°) using a GNR EXPLORER instrument (40 kV, 30 mA, and Cu-K α radiation); The size distribution was measured by a Dynamic light scattering (DLS) instrument (Microtrac, USA); Magnetic susceptibility measurements were measured using a vibrating sample magnetometer (VSM) BHV-55, Riken, Japan at room temperature; Thermal Gravimetric Analysis (TGA) was carried out using a TA-Q600. The TGA curve was obtained under an air atmosphere by heating at 10 °C/min from room temperature to 800 °C.

2.2. Preparation of magnetic (Fe_3O_4) nanospheres

A solution mixture containing $\text{FeCl}_3 \cdot 6\text{H}_2\text{O}$ (5.4 g) and $\text{FeCl}_2 \cdot 6\text{H}_2\text{O}$ (2.0 g) in 100 mL of deionized water was refluxed under nitrogen at 85 °C for 15 min. Then, 15 mL of an aqueous solution of ammonia (27%) was added dropwise and refluxed for 30 min. The mixture color immediately changed from orange to black. Finally, the magnetite precipitate (Fe_3O_4) was separated using a magnet and washed by deionized water three times (Tayeb et al., 2013). The prepared nanoparticles were finally characterized by FT-IR.

2.3. Preparation of magnetic-silica nanospheres ($\text{Fe}_3\text{O}_4@ \text{SiO}_2$)

The nanospheres were prepared according to a previous study with some modification. Briefly, a mixture of the synthesized Fe_3O_4 (3.0 g), TEOS (80 mL, 10% v/v), and glycerol (60 mL) having an adjusted pH value at 4.5 with acetic acid (AcOH) was refluxed at 90 °C for 2 h. The precipitate was separated using a magnet and washed by deionized water and methanol two times. The yield was dried at room temperature (Parvizi et al., 2019). The formation of nanoparticles was finally confirmed by FT-IR.

2.4. Preparation of magnetic-silica-vinyl nanospheres ($\text{Fe}_3\text{O}_4@ \text{SiO}_2@ \text{Vinyl}$)

A simple and reliable method was used for the preparation of the yield with slight modification (Zhang et al., 2016). Accordingly, $\text{Fe}_3\text{O}_4@ \text{SiO}_2$ (3.0 g) was suspended in ethanol (50 mL). Then, TMVS (10 mL) was added dropwise to the suspension. The pH was adjusted at 4.5 using AcOH. The mixture was then refluxed for 24 h and the obtained precipitate was separated using a magnet and washed by ethanol three times. The yield was dried in oven at 70 °C. FT-IR spectroscopy was used to identify the synthesized $\text{Fe}_3\text{O}_4@ \text{SiO}_2@ \text{Vinyl}$. Scheme 1 shows the sequential synthesis steps of $\text{Fe}_3\text{O}_4@ \text{SiO}_2@ \text{Vinyl}$.

2.5. Extraction of Psyllium hydrogel

The seeds of *P. ovata* (Psyllium) were purchased from a local herbal drug store in Sabzevar, Iran. At first, all foreign matter

such as dust, dirt, stones, and chaff were removed. To obtain Psyllium seeds husk, 50 g of its seeds was blended for 2 min. and then sieved (mesh 20). In the next step, 17 g of the husk was poured into 500 mL of deionized water and kept for 24 h at room temperature. Then, 1500 mL of ethanol (96 v/v %) was added to the hydrogel to separate the insoluble non-carbohydrate fractions of Psyllium seeds (PsyGel). All the aforementioned procedures were run for 3 times. Finally, the fraction was removed by filtration, washed with ethanol three times and the obtained product was put in a freeze dryer to dry for 72 h (Ladjevardi et al., 2015).

2.6. Preparation of $\text{Fe}_3\text{O}_4@ \text{SiO}_2@ \text{Vinyl} @ \text{PsyGel} @ \text{MFA}$ ($\text{Fe} / \text{POSH} / \text{MFA}$)

$\text{Fe}_3\text{O}_4@ \text{SiO}_2@ \text{Vinyl}$ (0.2 g) was completely dispersed in absolute ethanol (60 mL). Then, PsyGel-Vinyl (0.6 g) and MAA (102 μL) were added. The mixture was then placed in an ultrasonic bath for 15 min. In the next step, the mixture was stirred at 70 °C under nitrogen; after 12 h, EGDMA (230 μL), AIBN (2 mg), and MFA solution (1.0 g in 60 mL absolute ethanol) were added. The reaction mixture was refluxed under nitrogen for 24 h. Finally, The product was separated by a magnet, washed using acetic acid:methanol (9:1), and dried in an oven at 40 °C. EGDMA was used to form cross linkage between hydrogel and the magnetite core, while AIBN was utilized as the polymerization initiator. The final product was characterized by FT-IR and SEM techniques.

2.7. Swelling ratio of hydrogels

The swelling ratio of the Psyllium hydrogel was studied at different pHs (4.2, 7.4, and 9.0). For this propose, 1.0 g of the hydrogel was placed in the swelling medium (40 mL). After 1 h, the solvent was carefully removed; and the remaining hydrogel was weighed for 24 h at constant time intervals. The swelling ratio was calculated using the following formula for 3 times replications (Jeong et al., 2019):

$$\text{Swelling ratio (\%)} = [(W_{sh} - W_{dh}) / W_{dh}] \times 100 \quad (1)$$

where, W_{sh} and W_{dh} respectively account for the weight of swollen hydrogel (g) and the weight of dried hydrogel (g).

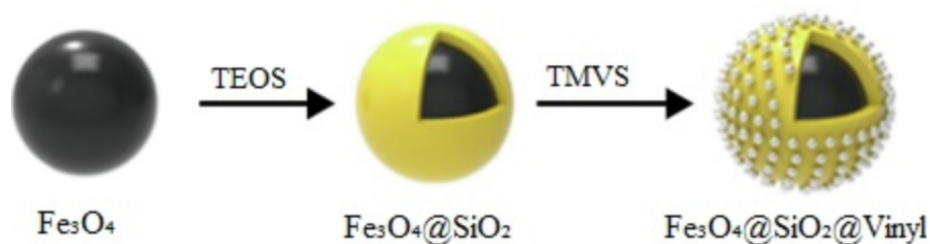
2.8. Preparation of PsyGel-Vinyl

To prepare PsyGel-Vinyl, 0.5 g of PsyGel in 50 mL of deionized water was stirred for 15 min. Then, 5 mL of TMVS was added to the mixture dropwise and refluxed for 24 h. The precipitate was separated and dried in oven at 60 °C. The yield was finally identified by FT-IR technique.

2.9. Drug encapsulation efficiency (DEE)

After washing the final product by methanol (three times), the concentration of the encapsulated drug was calculated using a standard curve of known MFA concentrations at 349 nm. The DEE was calculated using the following equation:

$$\text{Encapsulation efficiency (EE\%)} = [(m_1 - m_2) / m_1] \times 100 \quad (2)$$



Scheme 1 The synthesis steps and surface of $\text{Fe}_3\text{O}_4@SiO_2@Vinyl$.

where m_1 is the weight of MFA used for encapsulation and m_2 is the weight of encapsulated MFA.

2.10. Drug releasing evaluation (DRE)

A dialysis bag with a solution of Fe/POSH/MFA (0.2 g) in PBS (0.5 mL) was placed into a beaker containing 200 mL of PBS (pH 7.4). The releasing process was performed at 37 °C. At various times (after 1, 2, 4, 8, and 12 h), 2 mL- portions of the prepared mixture were withdrawn from the beaker to measure MFA absorbance at 349 nm and replaced with 2 mL of fresh PBS (Wang et al., 2013). The concentration of MFA was calculated regarding a standard curve of known MFA concentrations (1–75 $\mu\text{g}/\text{mL}$). The releasing evaluation was carried out for three times.

3. Results and discussion

3.1. XRD analysis

The crystallinity of Fe_3O_4 was evaluated using the relevant XRD pattern. In this sense, the corresponding diffractogram has been shown in Fig. 1a which confirms the synthesis of iron oxide that is consistent with FT-IR spectrum. As seen, the peaks at 2θ values of 30.27, 35.51, 43.48, 57.16, and 62.28 are indexed as (1 1 1), (3 1 1), (4 0 0), (5 1 1), and (4 4 0). The peak positions with 2θ values are in good agreement with those of magnetite (Fe_3O_4) obtained from standard database JCPDS No. 19-0629. The peaks at different degrees have also been previously reported (Yu and Kwak 2010). From the diffractogram, it is evident that the sample is clearly crystalline.

The XRD pattern of Fe/POSH/MFA is illustrated in Fig. 1b. Some differences are noted in this pattern compared to that of Fe_3O_4 . The baseline on the small angles of 2θ appears at higher intensity than those at higher angles. According to our experiences and previous reports, this is a common phenomenon when the metallic nanoparticles have been synthesized or coated by natural products (Mahdavi et al., 2019, Seydi et al., 2019, Ahmeda et al., 2020, Mahdavi et al., 2021, Zhang et al., 2021). On the other hand, the peak around 2θ of 21 shows the presence of Si in the Fe/POSH/MFA that has been reported previously (Liu et al., 2004, Tayebbe et al., 2015). The presence of broad peak at 19.47 and a peak at 31.09 can be related to Psyllium hydrogel (Mirzaei and Javanbakht 2019, Wadhera et al., 2020). The peaks at 14.2 and 26.3 related to the presence of MFA in the nanosphere that were also reported in some of the previously published reports (Ito et al., 2016).

3.2. Magnetic susceptibility measurements

The magnetic behaviors of Fe_3O_4 and the final product were evaluated using vibrating-sample magnetometer (VSM) (see Fig. 2a). In the absence of an external magnetic field, the magnetic moments of paramagnetic materials are randomly aligned. However, in the presence of a magnetic field, some of these moments will align, and the crystal will attain a small net magnetic moment. The magnetic materials that have no hysteresis loop, when being exposed to the external field are called superparamagnetic materials. The average size of these materials is usually lower than 100 nm (Teja and Koh 2009). According to the curve of the prepared Fe_3O_4 , the maximum saturation of particles magnetization is 70 emu/g; and there is no hysteresis loop for the material. Therefore, the synthesized Fe_3O_4 can be considered as superparamagnetic material.

The magnetic behavior of Fe/POSH/MFA was evaluated using VSM curve (Fig. 2b). As can be seen from this figure, the maximum saturation of particles magnetization is 25 emu/g. Obviously, coating of the synthetic Fe_3O_4 in the first step with a saturation value of 70 emu/g by the layers of silicate and hydrogel causes a decrease of saturation magnetization of Fe/POSH/MFA. However, the particles still retain superparamagnetic property, due to the absence of hysteresis loop.

3.3. SEM analysis

The surface morphology and size of Fe_3O_4 were investigated using field emission scanning electron microscope (FE-SEM) (Fig. 3 (a–d)). Fig. 3a and b depict the successful synthesis of iron oxide nanoparticles with spherical morphology and also imply uniformity, well dispersion and homogeneous characteristics of the prepared FeNPs. The diameter of particle size for FeNPs was in the range of 20–30 nm. Fig. 3c and d account for the formation of Fe/POSH/MFA with spherical morphology of the synthesized nanoparticles. Furthermore, the particles show a tendency for aggregation. The particle size of NPs was in the range of 40–50 nm. Compared to the size of Fe_3O_4 (20–30 nm), Fe/POSH/MFA is larger in size, which is due to coating of Fe_3O_4 by the layers of silicate and Psyllium hydrogel.

3.4. FT-IR spectra

3.4.1. FT-IR spectrum of Fe_3O_4

A simple and reliable co-precipitation method was used to synthesize Fe_3O_4 . To prevent the oxidation of the synthesized

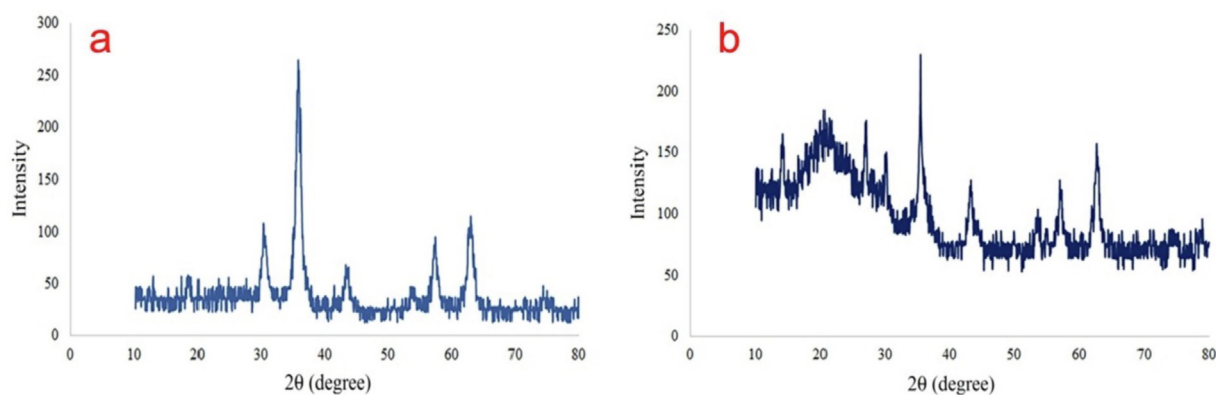


Fig. 1 The XRD diagram of Fe₃O₄(a) and Fe/POSH/MFA (b).

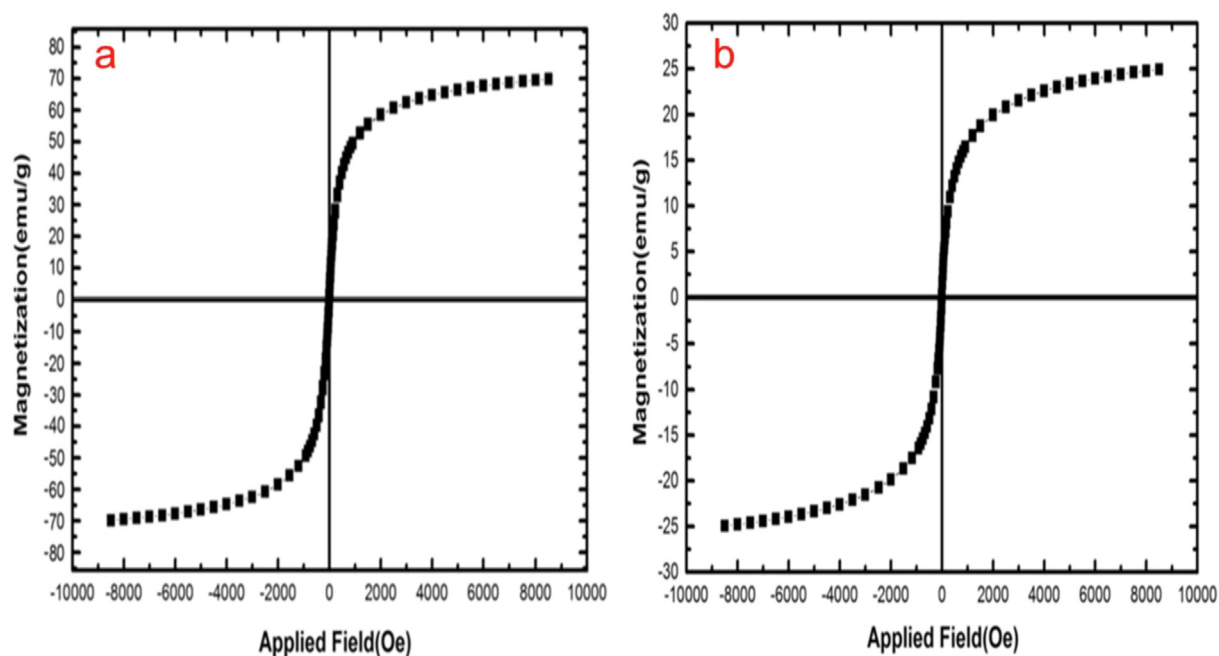


Fig. 2 Vibrating-sample magnetometer (VSM) curves (a. Fe₃O₄ and b. Fe/POSH/MFA).

nanoparticles, the procedure was performed under nitrogen atmosphere. The FT-IR spectrum of Fe₃O₄ is shown in Fig. 4a. The bands appearing at 430 and 560 cm⁻¹ respectively belong to Fe-O bond; and the peak at 3400 cm⁻¹ relates to OH on the surface of the synthesised Fe₃O₄.

3.4.2. FT-IR spectrum of Fe₃O₄@SiO₂

Oxidation and decomposition are the common problems encountered in the synthesis of FeNPs, mainly due to the environmental conditions (Saadati-Moshtaghin and Zonoz 2017). To avoid these shortcomings, the external surface of FeNPs was coated by a layer of SiO₂. To maintain the ability for surface functionalization, inhibition against further aggregation along with increasing of heat stability are the other advantages of silica coating of FeNPs (Gill et al., 2007). Scheme 2 illustrates the sequential steps of formation of functional groups at the surface of Fe₃O₄@SiO₂. The FT-IR spectrum of Fe₃O₄@SiO₂ confirms the preparation of the products (see Fig. 4b). In this relation, the band appearing at 3400 cm⁻¹ belongs to OH on the surface of nanoparticles and the peaks appearing at 980 and 1080 cm⁻¹ respectively belong to the symmetrical and asymmetrical stretching vibrations of Si—O—Si. The vibration band of Fe—O and Fe—O—Si appear around 460 cm⁻¹. The FT-IR spectrum of Fe₃O₄@SiO₂ is similar to those reported in the previous studies (Yamaura et al., 2004, Takami et al., 2007).

3.4.3. FT-IR spectrum of Fe₃O₄@SiO₂@Vinyl

3.4.3. FT-IR spectrum of Fe₃O₄@SiO₂@Vinyl

Scheme 3 shows the functionalized Fe₃O₄@SiO₂@Vinyl. The FT-IR spectroscopy is an efficient technique to characterize the chemical bindings on the surface of metallic nanoparticles. Hence, this method was used to approve the functionalization of Fe₃O₄@SiO₂ by TMVS. According to the FT-IR spectrum of Fe₃O₄@SiO₂@Vinyl (Fig. 4c), beside the peaks related to

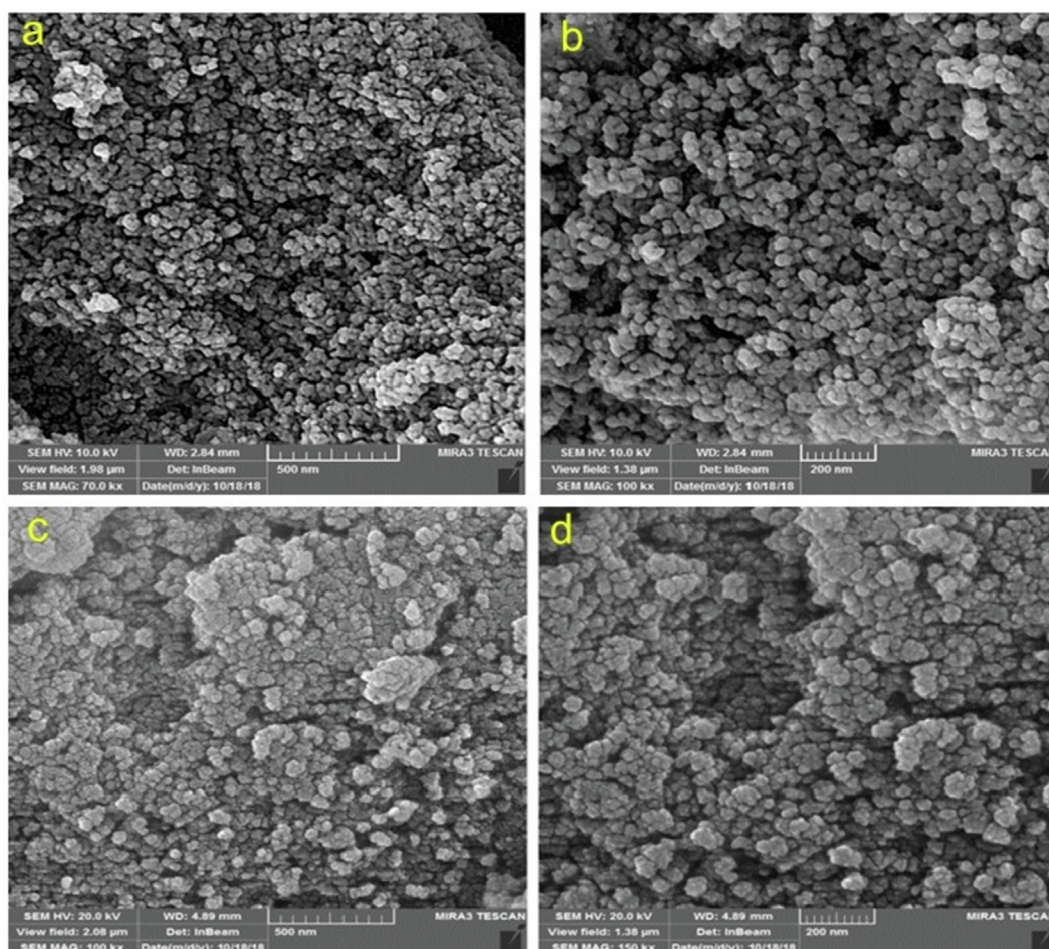


Fig. 3 The FE-SEM image of a,b. Fe_3O_4 ; c,d. Fe/POSH/MFA.

Si—O—Si, Fe—O—Si, and Fe—O, a new band appears at 1645 cm^{-1} that belongs to vibration of C=C bond of vinyl group.

3.4.4. FT-IR spectrum of Psyllium husk hydrogel

Arabinose, xylose, rhamnose, and galactose derivatives are the major components of Psyllium husk hydrogel (Kennedy et al., 1979, Fischer et al., 2004) and the relevant FT-IR spectrum has been shown in Fig. 5a. The band at 3400 cm^{-1} belongs to OH, the peak at 2925 cm^{-1} is assigned to CH, the bands at $1425\text{--}1608\text{ cm}^{-1}$ are respectively due to C=C and C=O, while peaks at $1328, 1258, 1103, 1045, 898, 714, 601, 533\text{ cm}^{-1}$ are attributed to polymer backbone. The peaks table is in full accordance with a previous report on FT-IR spectrum of Psyllium husk hydrogel (Saghir et al., 2008). The functional group of Psyllium husk hydrogel such as hydroxyl and carbonyl affect the increased drug loading capability (Atiyah et al., 2022).

3.4.5. FT-IR spectrum of mefenamic acid

Fig. 5b presents the FT-IR spectrum of mefenamic acid. A band at 1253 cm^{-1} belongs to C—O. The peaks from 1446 to 1600 cm^{-1} are assigned to aromatic C=C and C=O. In addition, the peak at 1647 cm^{-1} belongs to bending vibration of N—H. Finally, the peak at 3400 cm^{-1} accounts for the stretch-

ing vibration of N—H. The peaks are completely matched to the drug structure (Scheme 4) and previous reports (Ito et al., 2016, Antonio and Maggio 2018).

3.4.6. FT-IR spectrum of $\text{Fe}_3\text{O}_4@\text{SiO}_2@\text{Vinyl}@ \text{PsyGel}@ \text{MFA}$ (Fe/POSH/MFA)

The FT-IR spectrum of the final product is shown in Fig. 5c. The formation of Fe/POSH/MFA based on Psyllium hydrogel that comprises MFA is completely approved using FT-IR spectroscopy. The peak at 453 cm^{-1} confirms the presence of Fe—O bond; the bands at 760 and 1070 cm^{-1} belong to Si—O—Si bond; the peak at 1250 cm^{-1} is related to C—O bond that is found in the carbohydrate compounds of hydrogel; the peaks at $1434\text{--}1571\text{ cm}^{-1}$ are attributed to C=C in aromatic ring of MFA; the band at 2900 cm^{-1} is related to C—H bond; and the peak at 3308 cm^{-1} confirms the presence of N—H bond.

3.5. Thermal gravimetric analysis of Fe/POSH/MFA

Fig. 6 presents the thermal behavior of Fe/POSH/MFA at temperature range of $30\text{--}750\text{ }^\circ\text{C}$. According to this Figure, three areas with obvious loss of weight were detected in the TGA graph of the sample. The initially lost weight correlates to evaporation of adsorbed water at temperatures below

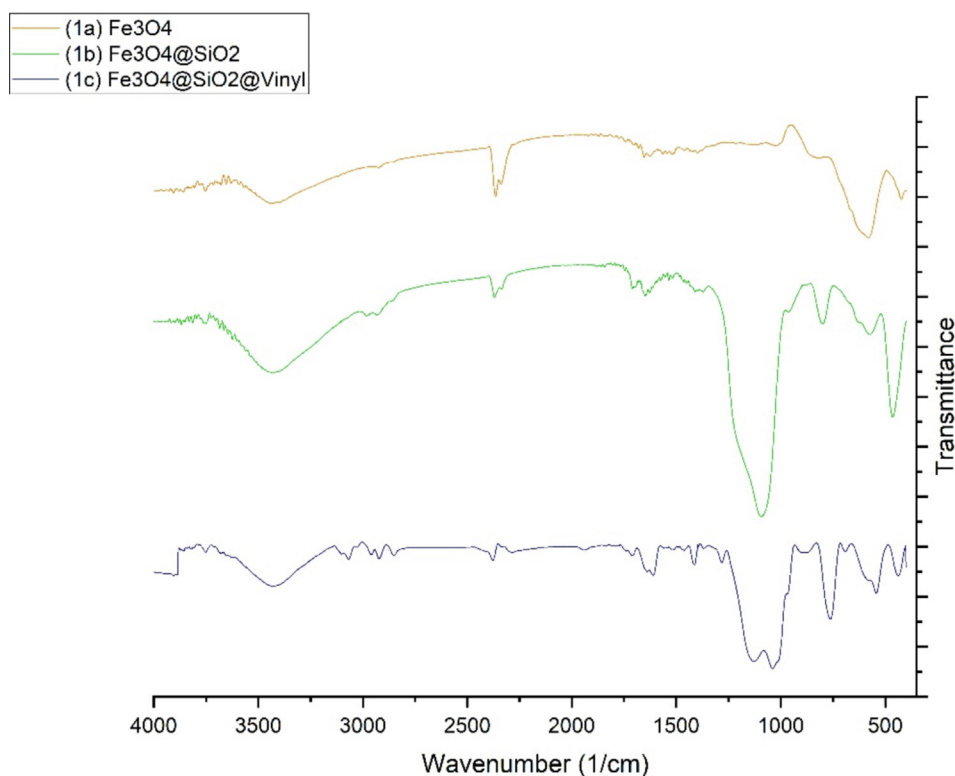
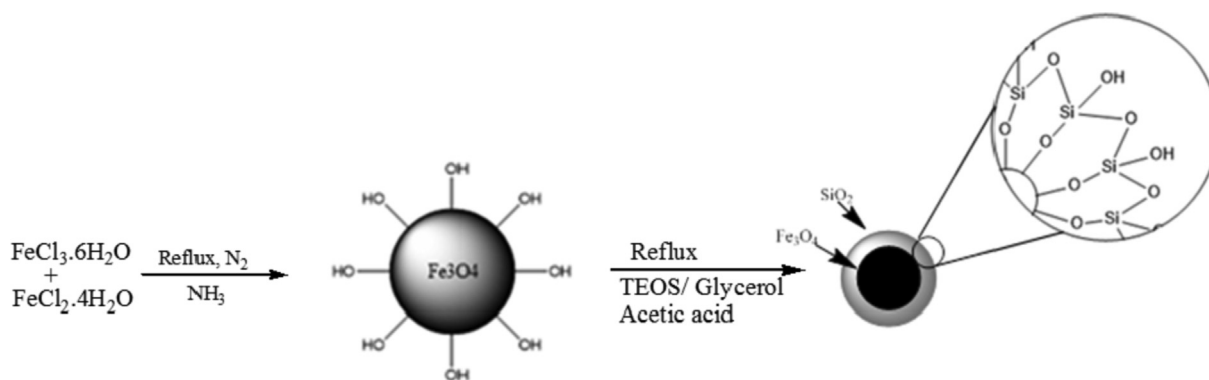


Fig. 4 The FT-IR spectra of the different yields of synthesis steps of magnetized core; 4a. for Fe_3O_4 ; 4b for $\text{Fe}_3\text{O}_4@\text{SiO}_2$; and 4c for $\text{Fe}_3\text{O}_4@\text{SiO}_2@\text{Vinyl}$.



Scheme 2 The synthesis steps and functional groups at the surface of $\text{Fe}_3\text{O}_4@\text{SiO}_2$.

100 °C. The next occurred at temperature range of 150–320 °C with a gradual decrease in slope and 15% loss of weight, and the third area appears at a temperature range of 320–450 °C. The last two weight losses can be associated to the combustion of organic molecules of Fe/POSH/MFA including MFA and Psyllium hydrogel.

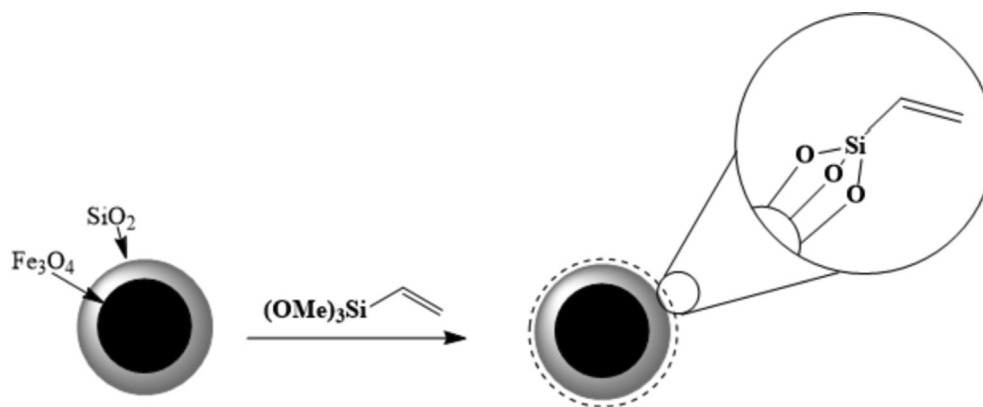
3.6. DLS analysis

The nanoparticles size is one of the most common factors that influences the biological behavior of NPs (Bhattacharjee 2016). Dynamic light scattering (DLS) is a familiar technique to determine the particle size of nanoparticles (Hoo et al., 2008). Accordingly, Fig. 7 shows the DLS analysis of the pre-

pared Fe/POSH/MFA. The maximum intensity is recorded for the size distribution less than 100 nm, which is the suitable size for nanoparticles to have interaction with cells such as inter-membrane transfer or contact release (Zou et al., 2014).

3.7. Swelling study of hydrogel

The swelling ability of the hydrogels is a key factor in drug delivery that influences the water sorption and drug release behaviors (Sharifzadeh et al., 2020). pH is one of the external factors that affects the swelling ratio. Moreover, the pH-sensitive hydrogels have been widely applied as drug delivery systems (Zhu et al., 2016). Fig. 8 illustrates the swelling behavior of Psyllium hydrogel at different pHs. The hydrogel exhi-



Scheme 3 The functionalization of the magnetized core of $\text{Fe}_3\text{O}_4@SiO_2@Vinyl$.

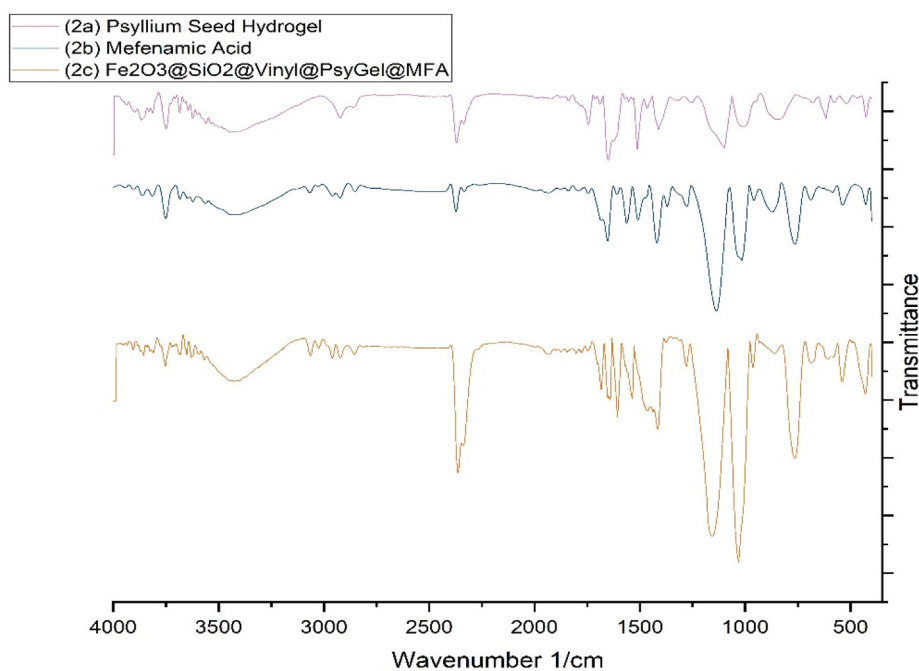
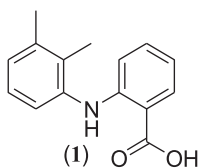


Fig. 5 The FT-IR spectra of 2a. Psyllium hydrogel; 2b. Mefenamic acid, and 2c. the nanosphere of $\text{Fe}_3\text{O}_4@SiO_2@Vinyl@PsyGel@MFA$ (Fe/POSH/MFA).



Scheme 4 The mefenamic acid structure.

bits a pH sensitivity behavior. The hydrogel swelling at acidic (pH = 4.2) and basic conditions (pH = 9.0) was less than pH 7.4. Our findings are in line with a previous study dealing with the measurement of the swelling behavior of Psyllium hydrogel at different pHs (Irfan et al., 2021). This study has reported the maximum swelling behavior at pH = 7.4. Since pH equal to 7.4 is very close to the human body pH, it can be concluded that Psyllium hydrogel is a sufficient mucilage for drug delivery

systems. Furthermore, this hydrogels type can be used to release the drug at a specific pH in a controlled manner (Jeong et al., 2019).

3.8. DEE and DRE

The presence of numerous functional groups and porous structures of hydrogels has been well documented as the main reason implying that hydrogels have excellent drug encapsulation and loading efficiencies (Jahanban-Esfahlan et al., 2020). The high measurable surface area and pore volumes, modifiable surfaces, non-toxicity, strong biocompatibility, and mesoporous particle morphology are affecting the release and loading on properties of the drug (Zhu et al., 2016). The DEE was calculated using Eq. (1) by which it was found to be 64.35%. To choose the best wavelength for DRE, the UV/Vis. spectra of the *psyllium* hydrogel and MFA were recorded. Taking into

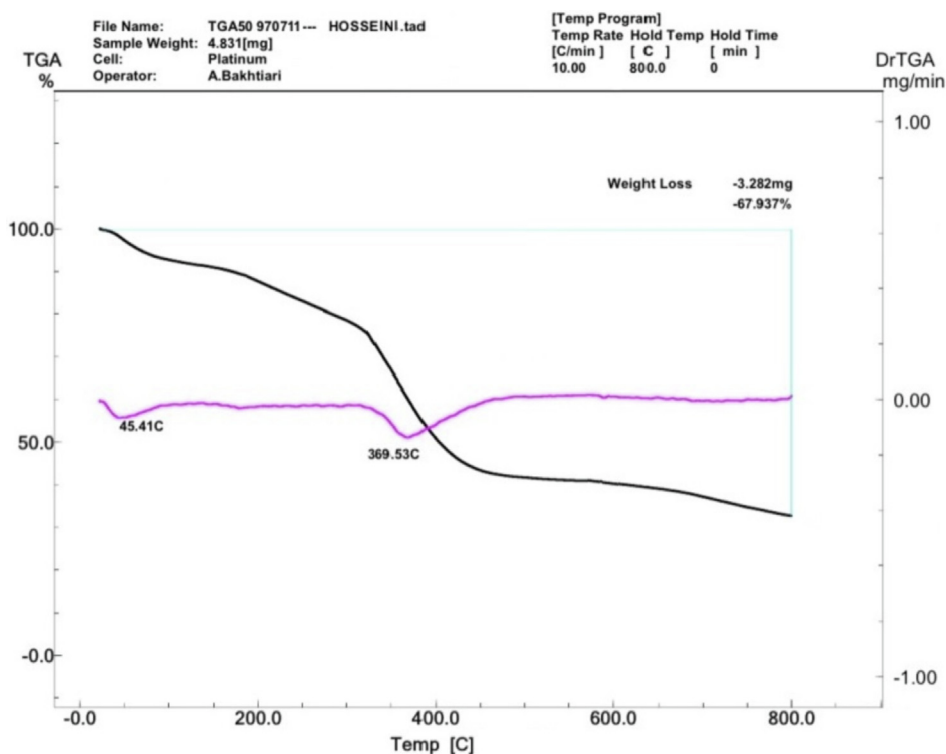


Fig. 6 Thermogravimetric analysis chart for Fe/POSH/MFA.

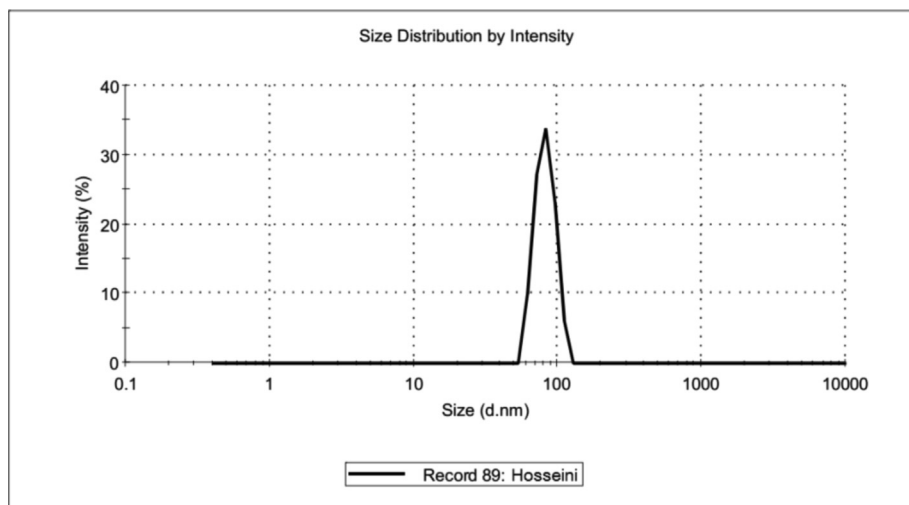


Fig. 7 The dynamic light scattering analysis (DLS) of Fe/POSH/MFA.

account the obtained spectra, the releasing trend was run at the wavelength of 394 nm, because the hydrogel did not show any absorbance at this selected wavelength. Fig. 9 shows the drug releasing of the prepared Fe/POSH/MFA. Since, drug release affects the drug efficacy of a drug delivery system, the release profile of MFA in the PBS was evaluated. According to the obtained results, $39.5 \pm 1.1\%$ of drug was released within the first 12 h. However, the release rate was then reduced until 24 h with the releasing amount of $52.7 \pm 2.05\%$. However, after this time, no significant release was observed for the drug. The maximum amount of drug releasing was recorded with value of $57.3 \pm 0.6\%$ for 72 h.

Some natural polymers, such as hydrogels, have been extensively investigated in encapsulated delivery systems. These systems are usually used to deliver therapeutic agents, drugs, and bioactive substances (Belščak-Cvitanović et al., 2015). Chitosan is one of the most popular natural polymers because of its unique properties (Nalini et al., 2019). On the other hand, the use of nanoparticles containing magnetic hydrogels has attracted increasing interest in the application of controlled drug delivery (Wang et al., 2013, Buhecha et al., 2019) in which the interaction between drug and hydrogel leads to sustaining drug releasing (Ghorpade et al., 2019, Jeong et al., 2019). This drug releasing retardation practically

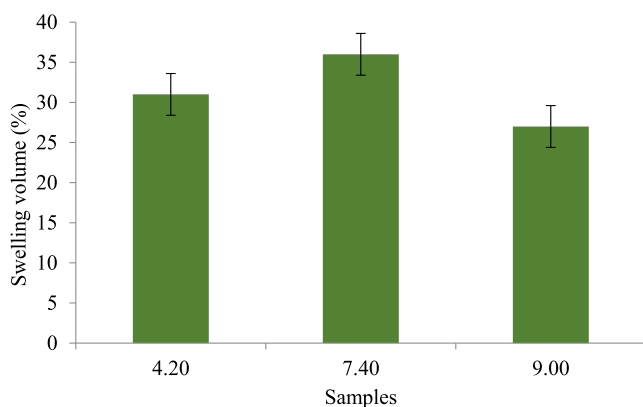


Fig. 8 The swelling behavior of Psyllium hydrogel at different pHs.

provides better interaction with biological materials, and possibly target drugs to specific organs or cells (Afrooz et al., 2017). The burst release is recognized as the mechanism of drug releasing from a distinct hydrogel (Ghorpade et al., 2019).

To initiate releasing process, drug molecules migrate from the initial position in the polymeric system to the polymer's outer surface and then to the release medium. Multiple factors, such as physicochemical properties of the solutes and structural characteristics of the material system afford this process (Miladi et al., 2015). Furthermore, the interaction of electrostatic attraction between the hydrogel and the drug, as well as hydrogen bonding, can affect the decrease of the drug primary burst release from nanohydrogels (Jafari et al., 2020). In the present study, the drug releasing of the magnetized

Psyllium hydrogel has been controlled by diffusion, swelling and erosion mechanism. Irfan et al. (Irfan et al., 2021) have reported this mechanism for the drug releasing of Psyllium hydrogel previously.

There are many reports in the literature dealing with the utilization of various drug delivery systems. In this context, Wu et al (2018) have reported the use of yeast as a carrier system to targeted drug delivery for doxorubicin in cancer therapy with a long retention time in the tumor tissue after intratumoral injection (Wu et al., 2018). The loading of alendronate in chitosan has been done by 70% for encapsulation efficiency with faster releasing at lower pH than PBS (pH = 6.8) (Miladi et al., 2015). Jeong et al (2019) have proposed the Fickian diffusion mechanism for the releasing of nobiletin from carboxymethyl chitosan (Jeong et al., 2019). Wang et al (2019) have prepared a magnetic carrier system for drug delivery of chelerythrine using a synthetic hydrogel of N-isopropylacrylamide and acrylamide. They have reported that the drug releasing depends on some experimental variables involving temperatures as well as the relevant alternating magnetic field (Wang et al., 2019). In another research, the releasing of budesonide and theophylline from an encapsulated system of polylactic acid showed a similar release profile over a period of 24 h at room temperature (Buhecha et al., 2019). The hydrogel microbeads based on sodium alginate has been found as an effective release system for drug delivery goals which represents high sensitivity to ultrasound for drug releasing (Kubota et al., 2021). A novel adhesive hydrogel of polyacrylamide/polydopamine serves as a strong carrier in transdermal drug delivery system (Jung et al., 2020). A comparison between our findings and previous reports on different drug delivery systems reveals that the Psyllium seed hydrogel is an effective carrier system for drug delivery due to the simplicity of

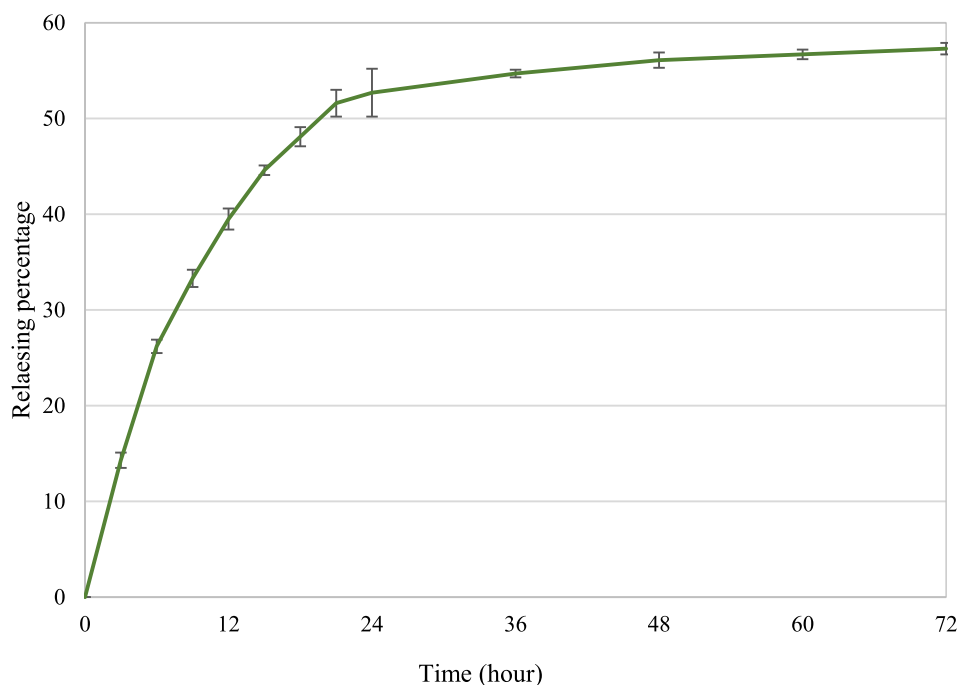


Fig. 9 Plot for the release amount of MFA in PBS solution.

hydrogel preparation, high ability of the hydrogel to drug loading, biodegradability, and its possibility for control drug releasing under different conditions.

4. Conclusion

In the current effort, Psyllium seeds hydrogel was magnetized using Fe_3O_4 to be utilized as a carrier system for the encapsulation of mefenamic acid as a reliable model in a targeted drug delivery system. The characterized system was found to be in nano size having spherical morphology. The size distribution of the system was also determined to be less than 100 nm with particles magnetization of 25 emu/g. The maximum releasing of 56%, after 72 h, was measured for *in vitro* drug releasing assay. Taking into account the findings of the present work, Psyllium hydrogel could be regarded as an efficient natural hydrogel in the targeted drug delivery system. However, further studies are still required to evaluate the challenges of loading of various drugs in this system. On the other hand, complementary *in vivo* studies may be conducted to investigate the safety of the proposed system as an effective nanocarrier for designing a potent drug delivery system.

CRedit authorship contribution statement

Behnam Mahdavi: Conceptualization, Methodology, Investigation, Resources, Writing – original draft, Visualization, Supervision, Project administration. **Sareh Hosseini:** Methodology, Investigation, Formal analysis, Software. **Majid Mohammadhosseini:** Data curation, Writing – review & editing. **Mohammad Mehrshad:** Methodology, Investigation, Validation.

Declaration of Competing Interest

The authors declare that they have no known competing financial interests or personal relationships that could have appeared to influence the work reported in this paper.

References

- Abukhadra, M.R., Refay, N.M., El-Sherbeeney, A.M., et al, 2020. Insight into the loading and release properties of MCM-48/biopolymer composites as carriers for 5-fluorouracil: equilibrium modeling and pharmacokinetic studies. *ACS Omega* 5, 11745–11755.
- Afroz, H., Ahmadi, F., Fallahzadeh, F., et al, 2017. Design and characterization of paclitaxel-verapamil co-encapsulated PLGA nanoparticles: potential system for overcoming P-glycoprotein mediated MDR. *J. Drug Delivery Sci. Technol.* 41, 174–181.
- Ahmadi, R., Kalbasi-Ashtari, A., Oromiehie, A., et al, 2012. Development and characterization of a novel biodegradable edible film obtained from Psyllium seed (*Plantago ovata* Forsk.). *J. Food Eng.* 109, 745–751.
- Ahmeda, A., Mahdavi, B., Zaker, F., et al, 2020. Chemical characterization and anti-hemolytic anemia potentials of tin nanoparticles synthesized by a green approach for bioremediation applications. *Appl. Organomet. Chem.* 34, e5433.
- Antonio, M., Maggio, R.M., 2018. Assessment of mefenamic acid polymorphs in commercial tablets using chemometric coupled to MIR and NIR spectroscopies. Prediction of dissolution performance. *J. Pharm. Biomed. Anal.* 149, 603–611.
- Atiyah, N.A., Albayati, T.M., Atiya, M.A., 2022. Functionalization of mesoporous MCM-41 for the delivery of curcumin as an anti-inflammatory therapy. *Adv. Powder Technol.* 103417.
- Belščak-Cvitanović, A., Komes, D., Karlović, S., et al, 2015. Improving the controlled delivery formulations of caffeine in alginate hydrogel beads combined with pectin, carrageenan, chitosan and Psyllium. *Food Chem.* 167, 378–386.
- Bhattacharjee, S., 2016. DLS and zeta potential—what they are and what they are not? *J. Control. Release* 235, 337–351.
- Boccardi, E., Liverani, L., Beltrán, A., et al, 2019. Mesoporous silica submicron particles (MCM-41) incorporating nanoscale Ag: synthesis, characterization and application as drug delivery coatings. *J. Porous Mater.* 26, 443–453.
- Brezoiu, A.-M., Deaconu, M., Nicu, I., et al, 2019. Heteroatom modified MCM-41-silica carriers for Lomefloxacin delivery systems. *Microporous Mesoporous Mater.* 275, 214–222.
- Buhecha, M.D., Lansley, A.B., Somavarapu, S., et al, 2019. Development and characterization of PLA nanoparticles for pulmonary drug delivery: co-encapsulation of theophylline and budesonide, a hydrophilic and lipophilic drug. *J. Drug Delivery Sci. Technol.* 53, 101128.
- Cheng, S., Zhang, C., Li, J., et al, 2021. Highly efficient removal of antibiotic from biomedical wastewater using Fenton-like catalyst magnetic pullulan hydrogels. *Carbohydr. Polym.* 262, 117951.
- Costa, J.A.S., de Jesus, R.A., Santos, D.O., et al, 2020. Recent progresses in the adsorption of organic, inorganic, and gas compounds by MCM-41-based mesoporous materials. *Microporous Mesoporous Mater.* 291, 109698.
- Fischer, M.H., Yu, N., Gray, G.R., et al, 2004. The gel-forming polysaccharide of Psyllium husk (*Plantago ovata* Forsk.). *Carbohydr. Res.* 339, 2009–2017.
- Ghorpade, V.S., Dias, R.J., Mali, K.K., et al, 2019. Citric acid crosslinked carboxymethylcellulose-polyvinyl alcohol hydrogel films for extended release of water soluble basic drugs. *J. Drug Delivery Sci. Technol.* 52, 421–430.
- Gill, C.S., Price, B.A., Jones, C.W., 2007. Sulfonic acid-functionalized silica-coated magnetic nanoparticle catalysts. *J. Catal.* 251, 145–152.
- Hoo, C.M., Starostin, N., West, P., et al, 2008. A comparison of atomic force microscopy (AFM) and dynamic light scattering (DLS) methods to characterize nanoparticle size distributions. *J. Nanopart. Res.* 10, 89–96.
- Iqbal, M.S., Akbar, J., Saghir, S., et al, 2011. Thermal studies of plant carbohydrate polymer hydrogels. *Carbohydr. Polym.* 86, 1775–1783.
- Irfan, J., Hussain, M.A., Haseeb, M.T., et al, 2021. A pH-sensitive, stimuli-responsive, superabsorbent, smart hydrogel from Psyllium (*Plantago ovata*) for intelligent drug delivery. *RSC Adv.* 11, 19755–19767.
- Ito, A., Konnerth, C., Schmidt, J., et al, 2016. Effect of polymer species and concentration on the production of mefenamic acid nanoparticles by media milling. *Eur. J. Pharm. Biopharm.* 98, 98–107.
- Iyer, S.R., Gogate, P.R., 2017. Ultrasound assisted crystallization of mefenamic acid: effect of operating parameters and comparison with conventional approach. *Ultrason. Sonochem.* 34, 896–903.
- Jafari, Z., Rad, A.S., Baharfar, R., et al, 2020. Synthesis and application of chitosan/tripolyphosphate/graphene oxide hydrogel as a new drug delivery system for Sumatriptan Succinate. *J. Mol. Liq.* 315, 113835.
- Jahanban-Esfahlan, R., Derakhshankhah, H., Haghshenas, B., et al, 2020. A bio-inspired magnetic natural hydrogel containing gelatin and alginate as a drug delivery system for cancer chemotherapy. *Int. J. Biol. Macromol.* 156, 438–445.
- Jarrar, Q.B., Ahmad, Z., Kadir, A.A., et al, 2017. Liposome encapsulation: a promising approach to enhanced and safe mefenamic acid therapy. *Int. Res. J. Educ. Sci.* 1, 32–39.
- Jeong, H.J., Nam, S.J., Song, J.Y., et al, 2019. Synthesis and physicochemical properties of pH-sensitive hydrogel based on carboxymethyl chitosan/2-hydroxyethyl acrylate for transdermal delivery of nobiletin. *J. Drug Delivery Sci. Technol.* 51, 194–203.

- Jiang, Y., Abukhadra, M.R., Refay, N.M., et al, 2020. Synthesis of chitosan/MCM-48 and β -cyclodextrin/MCM-48 composites as bio-adsorbents for environmental removal of Cd²⁺ ions; kinetic and equilibrium studies. *React. Funct. Polym.* 154, 104675.
- Jung, H., Kim, M.K., Lee, J.Y., et al, 2020. Adhesive hydrogel patch with enhanced strength and adhesiveness to skin for transdermal drug delivery. *Adv. Funct. Mater.* 30, 2004407.
- Kennedy, J.F., Sandhu, J.S., Southgate, D.A., 1979. Structural data for the carbohydrate of ispaghula husk ex *Plantago ovata* Forsk. *Carbohydr. Res.* 75, 265–274.
- Kubota, T., Kurashina, Y., Zhao, J., et al, 2021. Ultrasound-triggered on-demand drug delivery using hydrogel microbeads with release enhancer. *Mater. Des.* 203, 109580.
- Ladjevardi, Z.S., Gharibzadeh, S.M.T., Mousavi, M., 2015. Development of a stable low-fat yogurt gel using functionality of Psyllium (*Plantago ovata* Forsk) husk gum. *Carbohydr. Polym.* 125, 272–280.
- Liu, X., Ma, Z., Xing, J., et al, 2004. Preparation and characterization of amino-silane modified superparamagnetic silica nanospheres. *J. Magn. Magn. Mater.* 270, 1–6.
- Mahdavi, B., Saneei, S., Qorbani, M., et al, 2019. *Ziziphora clinopodioides* Lam leaves aqueous extract mediated synthesis of zinc nanoparticles and their antibacterial, antifungal, cytotoxicity, antioxidant, and cutaneous wound healing properties under in vitro and in vivo conditions. *Appl. Organomet. Chem.* 33, e5164.
- Mahdavi, B., Paydarfard, S., Rezaei-Seresht, E., et al, 2021. Green synthesis of NiONPs using *Trigonella subenervis* extract and its applications as a highly efficient electrochemical sensor, catalyst, and antibacterial agent. *Appl. Organomet. Chem.* 35, e6264.
- Miladi, K., Sfar, S., Fessi, H., et al, 2015. Enhancement of alendronate encapsulation in chitosan nanoparticles. *J. Drug Delivery Sci. Technol.* 30, 391–396.
- Mirzaei, S., Javanbakht, V., 2019. Dye removal from aqueous solution by a novel dual cross-linked biocomposite obtained from mucilage of *Plantago* Psyllium and eggshell membrane. *Int. J. Biol. Macromol.* 134, 1187–1204.
- Nalini, T., Basha, S.K., Sadiq, A.M.M., et al, 2019. Development and characterization of alginate/chitosan nanoparticulate system for hydrophobic drug encapsulation. *J. Drug Delivery Sci. Technol.* 52, 65–72.
- Pan, X., Cheng, S., Zhang, C., et al, 2021. Mussel-inspired magnetic pullulan hydrogels for enhancing catalytic degradation of antibiotics from biomedical wastewater. *Chem. Eng. J.* 409, 128203.
- Parvizi, E., Tayebee, R., Koushki, E., et al, 2019. Photocatalytic efficacy of supported tetrazine on MgZnO nanoparticles for the heterogeneous photodegradation of methylene blue and ciprofloxacin. *RSC Adv.* 9, 23818–23831.
- Porrang, S., Rahemi, N., Davaran, S., et al, 2021. Synthesis of temperature/pH dual-responsive mesoporous silica nanoparticles by surface modification and radical polymerization for anti-cancer drug delivery. *Colloids Surf., A* 623, 126719.
- Qi, X., Huang, Y., You, S., et al, 2022. Engineering robust Ag-decorated polydopamine nano-photothermal platforms to combat bacterial infection and prompt wound healing. *Adv. Sci.* 9, 2106015.
- Saadati-Moshtaghin, H.R., Zonoz, F.M., 2017. Preparation and characterization of magnetite-dihydrogen phosphate as a novel catalyst in the synthesis of tetrahydrobenzo [b] pyrans. *Mater. Chem. Phys.* 199, 159–165.
- Saghir, S., Iqbal, M.S., Hussain, M.A., et al, 2008. Structure characterization and carboxymethylation of arabinoxylan isolated from Ispaghula (*Plantago ovata*) seed husk. *Carbohydr. Polym.* 74, 309–317.
- Seydi, N., Mahdavi, B., Paydarfard, S., et al, 2019. Preparation, characterization, and assessment of cytotoxicity, antioxidant, antibacterial, antifungal, and cutaneous wound healing properties of titanium nanoparticles using aqueous extract of *Ziziphora clinopodioides* Lam leaves. *Appl. Organomet. Chem.* 33, e5009.
- Sharifzadeh, G., Hezaveh, H., Muhamad, I.I., et al, 2020. Montmorillonite-based polyacrylamide hydrogel rings for controlled vaginal drug delivery. *Mater. Sci. Eng., C* 110, 110609.
- Takami, S., Sato, T., Mousavand, T., et al, 2007. Hydrothermal synthesis of surface-modified iron oxide nanoparticles. *Mater. Lett.* 61, 4769–4772.
- Tantiwattanakul, P., Taneepanichskul, S., 2004. Effect of mefenamic acid on controlling irregular uterine bleeding in DMPA users. *Contraception* 70, 277–279.
- Tayebee, R., Amini, M.M., Abdollahi, N., et al, 2013. Magnetic inorganic-organic hybrid nanomaterial for the catalytic preparation of bis (indolyl) arylmethanes under solvent-free conditions: preparation and characterization of H5PW10V2O40/pyridino-Fe3O4 nanoparticles. *Appl. Catal. A* 468, 75–87.
- Tayebee, R., Amini, M., Akbari, M., et al, 2015. A novel inorganic-organic nanohybrid material H 4 SiW 12 O 40/pyridino-MCM-41 as efficient catalyst for the preparation of 1-amidoalkyl-2-naphthols under solvent-free conditions. *Dalton Trans.* 44, 9596–9609.
- Teja, A.S., Koh, P.-Y., 2009. Synthesis, properties, and applications of magnetic iron oxide nanoparticles. *Prog. Cryst. Growth Charact. Mater.* 55, 22–45.
- Vareda, J.P., Matias, T., Durães, L., 2018. Facile preparation of ambient pressure dried aerogel-like monoliths with reduced shrinkage based on vinyl-modified silica networks. *Ceram. Int.* 44, 17453–17458.
- Wadhwa, P., Jindal, R., Dogra, R., 2020. Insight into adsorption kinetics and isotherms for adsorption of methylene blue using gum rosin alcohol/Psyllium-based green adsorbent. *Iran. Polym. J.* 29, 501–514.
- Wang, C., Mallela, J., Garapati, U.S., et al, 2013. A chitosan-modified graphene nanogel for noninvasive controlled drug release. *Nanomed.: Nanotechnol. Biol. Med.* 9, 903–911.
- Wang, Y.-H., Zhong, M., Wang, L., et al, 2019. Chelerythrine loaded composite magnetic thermosensitive hydrogels as a novel anti-cancer drug-delivery system. *J. Drug Delivery Sci. Technol.* 54, 101293.
- Wu, Y., Zhong, C., Du, T., et al, 2018. Preparation and characterization of yeast-encapsulated doxorubicin microparticles. *J. Drug Delivery Sci. Technol.* 45, 442–448.
- Yamaura, M., Camilo, R., Sampaio, L., et al, 2004. Preparation and characterization of (3-aminopropyl) triethoxysilane-coated magnetite nanoparticles. *J. Magn. Magn. Mater.* 279, 210–217.
- Yu, B.Y., Kwak, S.-Y., 2010. Assembly of magnetite nanocrystals into spherical mesoporous aggregates with a 3-D wormhole-like pore structure. *J. Mater. Chem.* 20, 8320–8328.
- Yu, L., Yakubov, G.E., Zeng, W., et al, 2017. Multi-layer mucilage of *Plantago ovata* seeds: rheological differences arise from variations in arabinoxylan side chains. *Carbohydr. Polym.* 165, 132–141.
- Yuan, S., Wang, M., Liu, J., et al, 2020. Recent advances of SBA-15-based composites as the heterogeneous catalysts in water decontamination: a mini-review. *J. Environ. Manage.* 254, 109787.
- Zauska, L., Bova, S., Benova, E., et al, 2021. Thermosensitive drug delivery system SBA-15-PEI for controlled release of nonsteroidal anti-inflammatory drug diclofenac sodium salt: a comparative study. *Materials* 14, 1880.
- Zhang, Y., Mahdavi, B., Mohammadhosseini, M., et al, 2021. Green synthesis of NiO nanoparticles using *Calendula officinalis* extract: Chemical characterization, antioxidant, cytotoxicity, and anti-esophageal carcinoma properties. *Arab. J. Chem.* 14, 103105.
- Zhang, C., Yu, J., Feng, K., et al, 2016. Synthesis and characterization of triethoxyvinylsilane surface modified layered double hydroxides and application in improving UV aging resistance of bitumen. *Appl. Clay Sci.* 120, 1–8.
- Zhu, G., Zhang, Y., Wang, K., et al, 2016. Visualized intravesical floating hydrogel encapsulating vaporized perfluoropentane for controlled drug release. *Drug Delivery* 23, 2820–2826.

Zisimopoulos, E.G., Tsogas, G.Z., Giokas, D.L., et al, 2009. Indirect chemiluminescence-based detection of mefenamic acid in pharmaceutical formulations by flow injection analysis and effect of gold nanocatalysts. *Talanta* 79, 893–899.

Zou, L.-Q., Liu, W., Liu, W.-L., et al, 2014. Characterization and bioavailability of tea polyphenol nanoliposome prepared by combining an ethanol injection method with dynamic high-pressure microfluidization. *J. Agric. Food. Chem.* 62, 934–941.